Diapycnal mixing across the photic zone of the NE-Atlantic

by Hans van Haren*, Corina P.D. Brussaard, Loes J. A. Gerringa, Mathijs H. van Manen, Rob Middag, Ruud Groenewegen

Royal Netherlands Institute for Sea Research (NIOZ), P.O. Box 59, 1790 AB Den Burg, the Netherlands.
*e-mail: hans.van.haren@nioz.nl

Abstract. Variable physical conditions such as vertical turbulent exchange, internal wave and mesoscale eddy action, affect the availability of light and nutrients for phytoplankton (unicellular algae) growth. It is hypothesized that changes in ocean temperature may affect ocean vertical density stratification, which may hamper vertical exchange. In order to quantify variations in physical conditions in the Northeast Atlantic Ocean, we sampled a latitudinal transect along 17±5°W between 30 and 63°N in summer. A shipborne Conductivity-Temperature-Depth CTD-instrumented package was used with a custom-made modification of the pump-inlet to minimize detrimental effects of ship motions on its data. Thorpe-scale analysis was used to establish turbulence values for the upper 500 m from 3 to 6 profiles obtained in a short CTD-yoyo, 3 to 5 h after local sunrise. From south to north, average temperature decreased together with stratification while turbulence values weakly increased or remained constant. Vertical turbulent nutrient fluxes did not vary significantly with stratification and latitude. This apparent lack of correspondence between turbulent mixing and temperature is likely due to internal waves breaking (increased stratification can support more internal waves), acting as a potential feed-back mechanism. As this feed-back mechanism mediates potential physical environment changes in temperature, global surface ocean warming may not affect the vertical nutrient fluxes to a large degree. We urge modelers to test this deduction as it could imply that the future summer phytoplankton productivity in stratified oligotrophic waters would experience little alterations in nutrient input from deeper waters.

1 Introduction

The physical environment is important for ocean life, including variations therein. For example, the sun stores heat in the ocean with a stable vertical density stratification as result. Generally, stratification hampers vertical turbulent exchange because of the required work against (reduced) gravity before turbulence can take effect. It thus hampers a supply of nutrients via a turbulent flux from deeper waters to the photic zone. However, stratification supports internal waves, which (i) may move near-floating particles like phytoplankton (unicellular algae) up- and down towards and away from the surface, and (ii) may induce enhanced turbulence via vertical current differences (shear) resulting in internal waves breaking (Denman and Gargett, 1983). Such changes in the physical environment are expected to affect the availability of phytoplankton growth factors such as light and nutrients**.**

Climate models predict that global warming will reduce vertical mixing in the oceans (e.g., Sarmiento et al., 2004). Mathematical models on system stability suggest that reduced mixing may generate chaos behaviour in phytoplankton production, thereby enhancing variability in carbon export into the ocean interior (Huisman et al., 2006). However, none of these models include potential feed-back systems like internal wave action or mesoscale eddy activity. From observations in the relatively shallow North Sea it is known that the strong seasonal temperature stratification is marginally stable, as it supports internal waves and shear to such extent that sufficient nutrients are replenished from below to sustain the late-summer phytoplankton bloom in the euphotic zone that became depleted of nutrients after the spring bloom (van Haren et al., 1999). This challenges the current paradigm in climate models.

In this paper, the objective is to resolve the effect of vertical stratification and turbulent mixing on nutrient supply to the euphotic zone of the open ocean. For this purpose, upper-500-m-ocean shipborne Conductivity-Temperature-Depth CTD-observations were made in association with those on dissolved inorganic nutrients during a survey along a transect in the NE-Atlantic Ocean from mid-(30°) to high--(63°) latitudes in summer. Throughout the survey, meteorological and sea-state conditions were favourable for adequate sampling and wind

92 speeds varied little between 5 and 10 m s^{-1}, independent of locations. All CTD-observations
93 were made far from lateral, continental boundaries and at least 1000 m vertically away from
94 bottom topography (i.e. far from internal-tide sources). The NE-Atlantic is characterized by
95 abundant (sub-)mesoscale eddies especially in the upper ocean (Charria et al., 2017) that
96 influence local plankton communities (Hernández- Hernández et al., 2020). The area also
97 shows continuous abundant internal wave activity away from topographic sources and sinks,
98 with the semidiurnal tide as a main source from below and atmospherically induced inertial
99 motions from above (e.g., van Haren, 2005; 2007). However, the sampled upper 500-m zone
100 transect is not known to demonstrate outstanding internal wave source variations. Previous
101 observations (van Haren, 2005) and Hibiya et al. (2007) have shown that a diurnal critical
102 latitude enhancement of near-inertial internal waves due to subharmonic instability only occurs
103 sharply between 25 and 30°N. The present observations are all made poleward of this range.
104 Likewise, the Henyey et al. (1986) model on latitudinal variation of internal wave energy and
105 turbulent mixing (Gregg et al., 2003) predicts changes by a factor of maximum 1.8 between
106 30° and 63°, but this value is relatively small compared with errors, typically a factor of 2 to 3,
107 in turbulence dissipation rate observations. Likewise, from the equal summertime
108 meteorological conditions little variation is expected in the generation of upper ocean near-
109 inertial internal waves. Naturally, other processes like interaction between internal waves and
110 mesoscale phenomena may be important locally, but these are expected to occur in a similar
111 fashion across the sampled ocean far away from boundaries. Thus, the sampled dataset is
112 considered adequate for a discussion on the variability of turbulence, stratification and vertical
113 turbulent nutrient fluxes with latitude.

114 The present research complements research based on photic zone (upper 100 m)
115 observations obtained along the same transect using a slowly descending turbulence
116 microstructure profiler next to CTD-sampling eight years earlier (Jurado et al., 2012). Their
117 data demonstrated a negligibly weak increase in turbulence values with significant decreases in
118 stratification going north. However, no nutrient data were presented and no turbulent nutrient

fluxes could be computed. In another summertime study (Mojica et al., 2016), macro-nutrient concentrations indicated oligotrophic conditions along the same latitudinal transect but the vertical gradients for the upper 200 m showed an increase from south to north. The present observations go deeper to 500 m, also across the non-seasonal more permanent stratification. Moreover, coinciding measurements were made of the distributions of macro-nutrients and dissolved iron. This allows vertical turbulent nutrient fluxes to be computed. It leads to a hypothesis concerning a physical feed-back mechanism that may control changes in stratification.

2 Materials and Methods

Between 22 July and 16 August 2017, observations were made from the R/V Pelagia in the Northeast Atlantic Ocean at stations along a transect from Iceland, starting around 60°N, to the Canary Islands, ending at 30°N, (Fig. 1). The transect was roughly in meridional direction, with stations along 17±5°W, all in the same time zone (UTC-1 h = local time LT). Full water-depth Rosette bottle water sampling was performed at most stations.

Samples for dissolved inorganic macro-nutrients were filtered through 0.2 μm Acrodisc filter and stored frozen in a high-density polyethylene pony-vial (nitrate, nitrite and phosphate) or at 4ºC (silicate) until analysis. Nutrients were analysed under temperature controlled conditions using a QuAAtro Gas Segmented Continuous Flow Analyser. All measurements were calibrated with standards diluted in low nutrient seawater in the salinity range of the stations to ensure that analysis remained within the same ionic strength. Phosphate (PO_4), nitrate plus nitrite (NO_x), were measured according to Murphy and Riley (1962) and Grasshoff et al. (1983), respectively. Silicate was analysed using the procedure of Strickland and Parsons (1968).

Absolute and relative precision were regularly determined for reasonably high concentrations in an in-house standard. For phosphate, the standard deviation was 0.028 μM (N = 30) for a concentration of 0.9 μM; Hence the relative precision was 3.1%. For nitrate, the

values were 0.14 μM (N = 30) for a concentration of 14.0 μM, so that the relative precision was 1.0%. For silicate, the values were 0.09 μM (N = 15) for a concentration of 21.0 μM, so that the relative precision was 0.4%. The detection limits were 0.007, 0.012 and 0.008 μM, for phosphate, nitrate and silicate, respectively.

For dissolved iron samples, the ultraclean "Pristine" sampling system for trace metals was used (Rijkenberg et al., 2015). All bottles used for storage of reagents and samples were cleaned according to an intensive three step cleaning protocol described by Middag et al. (2009). Dissolved iron concentrations were measured shipboard using a Flow Injection—Chemiluminescence method with preconcentration on iminodiaceticacid resin as described by De Baar et al. (2008) and modified by Klunder et al. (2011). In order to validate the accuracy of the system, standard reference seawater (SAFe) was measured regularly in triplicate (Johnson et al. 1997).

At 19 out of 32 stations a yoyo consisting of 3 to 6 casts, totaling 72 casts, of electronic CTD profiles was done to monitor the temperature-salinity variability and to establish turbulent mixing values from 5 to 500 m below the ocean surface. The yoyo casts were made consecutively and took between 1 and 2 hours per station. They were mostly obtained in the morning: at ten stations between 6 and 8 LT, at eight stations between 8 and 10 LT, and at one station in the afternoon, around noon. As the observations were made in summer, the latitudinal difference in sunrise was 1.5 h between the northernmost (earlier sunrise) and southernmost stations. This difference is taken into account and sampling times are referenced to time after local sunrise. It is assumed that the stations sampled just after sunrise reflect the upper ocean conditions of (late-) nighttime cooling convection so that vertical near-homogeneity was at a maximum, and near-surface stratification at a minimum, while the late morning and afternoon stations reflected daytime stratifying near-surface conditions due to the stabilizing solar insolation.

173 **2.1 Instrumentation and modification**

174 A calibrated SeaBird 911plus CTD was used. The CTD data were sampled at a rate of 24
175 Hz, whilst lowering the instrumental package at a speed of 1 m s^{-1}. The data were processed
176 using the standard procedures incorporated in the SBE-software, including corrections for cell
177 thermal mass (Lueck, 1990) using the parameter setting of Mensah et al. (2009) and sensor
178 time-alignment. All other analyses were performed using Conservative Temperature (Θ),
179 Absolute Salinity S_A and potential density anomalies σ_θ, with 1000 kg m^{-3} subtracted from total
180 density and referenced to the surface for pressure corrections as vertical profiles were only
181 analyzed shallower than 600 m, using the Gibbs SeaWater-software (IOC, SCOR, IAPSO,
182 2010).

183 Observations were made with the CTD upright rather than horizontal in a lead-weighted
184 frame without water samplers to minimize artificial turbulent overturning. Variable speeds of
185 the flow passing the temperature and conductivity sensors will cause artificial temperature and
186 thus apparent turbulent overturning, noticeable in near-homogeneous waters such as found near
187 the surface during nighttime convection. To eliminate variable flow speeds, a custom-made
188 assembly with pump in- and outlet tubes and tube-ends of exactly the same diameter was
189 mounted to the CTD as described in van Haren and Laan (2016). This reduces frictional
190 temperature effects of typically ±0.5 mK due to fluctuations in pump speed of ±0.5 m s^{-1} when
191 standard SBE-tubing is used (Appendix A1). The effective removal of the artificial temperature
192 effects using the custom-made assembly is demonstrated in Fig. 2, in which surface wave action
193 via ship motion is visible in the CTD-pressure record, but not in its temperature variations
194 record. For example, at station 32 the CTD was lowered in moderate sea state conditions with
195 surface waves of maximum 2 m crest-trough. The surface waves are recorded by pressure
196 variations as a result of ship motions (Fig. 2a). In the upper 35 m near the surface, the waters
197 were partially unstable and partially near-homogeneous, with temperature variations well
198 within ±0.5 mK and high-frequency variations O(0.1) mK (Fig. 2b). The ΔT-variations did not
199 vary with the surface wave periodicity of about 10 s. No correlation was found between data in

Fig. 2b and Fig. 2a. This effective removal of ship motion in CTD-temperature data is confirmed for the entire 500 m depth-range in average spectral information (Fig. 2c-e). In the power spectra, the pressure gradient dp/dt ~ CTD-velocity shows a clear peak around 0.1 cps, short for cycles per s, which correspond to a period of 10 s. Such a peak is absent in both spectra of temperature T and density anomaly referenced to the surface σ_θ. The correlation between dp/dt and T is not significantly different from zero (Fig. 2d,e). With conventional tubing and tube-ends, the surface wave variations would show in such ΔT-graph (van Haren and Laan, 2016). Without the effects of ship motions, considerably less corrections need to be applied for turbulence calculations (see below).

2.2 Ocean turbulence calculation

Turbulence is quantified using the analysis method by Thorpe (1977) on potential density inversions of less dense water below a layer of denser water in a vertical (z) profile. Such inversions are interpreted as turbulent overturns of mechanical energy mixing. Vertical turbulent kinetic energy dissipation rate (ε) is a measure of the amount of kinetic energy put in a system for turbulent mixing. It is proportional to the magnitude of turbulent diapycnal flux (of potential density) $|K_z d\sigma_\theta/dz|$. In practice it is determined by calculating overturning scales with magnitude |d|, just like turbulent eddy diffusivity (K_z). The vertical potential density stratification is indicated by $d\sigma_\theta/dz$. The turbulent overturning scales are obtained after reordering the measured profile $\sigma_\theta(z)$, which may contain inversions, into a stable monotonic profile $\sigma_\theta(z_s)$ without inversions (Thorpe, 1977). After comparing raw and reordered profiles, displacements $d = \min(|z-z_s|)\cdot\mathrm{sgn}(z-z_s)$ are calculated that generate the stable profile. Then, using root-mean-square displacement value $L_T = \mathrm{rms}(d)$ computed over certain vertical scales (see below),

$$\varepsilon = 0.64 L_T^2 N^3 \qquad [m^2 s^{-3}], \tag{1}$$

where $N = \{-g/\rho(d\sigma_\theta(z_s)/dz\}^{1/2}$ denotes the buoyancy frequency (~ square-root of stratification as is clear from the equation) computed from the reordered profile. Here, g is the acceleration

of gravity and ρ = 1027 kg m^{-3} denotes the reference density. We like to note, following previous warnings by, e.g., Gill (1982) and King et al. (2012), that our definition of N is a practical one, which should not be used for data from deeper waters. For deeper waters, density should be referenced to a local pressure reference level, which effectively implies the use of the exact definition for buoyancy frequency as formulated, e.g., by Gill (1982): $\{-g/\rho(d\rho/dz + g\rho/c_s^2\}^{1/2}$, where c_s is the speed of sound reflecting pressure-compressibility effects. Our 'surface waters' N computed over reordered profiles only negligibly deviates from above exact N and corresponds with N computed from raw profiles over a typical vertical length-scale of Δz = 100 m. This Δz represents the scales of large internal waves that are supported by the density stratification and of the largest turbulent overturns.

The numerical constant of 0.64 in (1) follows from empirically relating the overturning scale magnitude with the Ozmidov scale L_O of largest possible turbulent overturn in a stratified flow: $(L_O/L_T) = 0.8$ (Dillon, 1982), a mean coefficient value from many realizations. Using $K_z = \Gamma\varepsilon N^{-2}$ and a mean mixing efficiency coefficient of $\Gamma = 0.2$ for the conversion of kinetic into potential energy for ocean observations that are suitably averaged over all relevant turbulent overturning scales of the mix of shear-, current differences, and convective, buoyancy driven, turbulent overturning in large Reynolds number flow conditions (e.g., Osborn, 1980; Oakey, 1982; Ferron et al., 1998; Gregg et al., 2018), we find,

$$K_z = 0.128 L_T^2 N \qquad [m^2 s^{-1}]. \tag{2}$$

This parametrization is also valid for the upper ocean, as has been shown extensively by Oakey (1982) and recently confirmed by Gregg et al. (2018). The inference is that the upper ocean may be weakly stratified at times, but stratification and turbulence vary considerably with time and space. Sufficient averaging collapses coefficients to the mean values given above. This is confirmed in recent numerical modeling by Portwood et al. (2019).

As K_z is a mechanical turbulence coefficient it is not property-dependent like a molecular diffusion coefficient that is about 100-fold different for temperature compared to salinity. K_z is thus the same for all turbulent transport calculations no matter what gradient of what property.

For example, the vertical downgradient turbulent flux of dissolved iron transporting from iron-rich deeper waters upwards into the euphotic zone is computed as $-K_z d(DFe)/dz$.

According to Thorpe (1977), results from (1) and (2) are only useful after averaging over the size of a turbulent overturn instead of using single displacements. Here, rms-displacement values L_T are not determined over individual overturns, as in Dillon (1982), but over 7 m vertical intervals (equivalent to about 200 raw data samples) that just exceed average L_O. This avoids the complex distinction of smaller overturns in larger ones and allows the use of a single length scale of averaging. As a criterion for determining overturns we only used those data of which the absolute value of difference with the local reordered value exceeds a threshold of 7×10^{-5} kg m^{-3}, which comes from standard deviations of the potential density profiles in near-homogeneous layers over 1-m intervals and which corresponds to noise-variational amplitudes of 1.4×10^{-4} kg m^{-3} in raw data (e.g., Galbraith and Kelley, 1996; Stansfield et al., 2001; Gargett and Garner, 2008). Vertically averaged turbulence values, short for averaged ε- and K_z-values from (1) and (2), can be calculated to within an error of a factor of two to three, approximately. As will be demonstrated below, this is considerably less spread in values than the natural turbulence values variability over typically four orders of magnitude at a given position and depth in the ocean (e.g., Gregg, 1989).

3 Results

3.1 Physical parameters

An early morning vertical profile of density anomaly in the upper 500 m at a northern station (Fig. 3a) is characterized by a near-homogeneous layer of about 15 to 40 m, which is above a layer of relatively strong stratification and a smooth moderate stratification deeper below. In the near-homogeneous upper layer, in this example $z > -30$ m, relatively large turbulent overturn displacements can be found of $d = \pm 20$ m (Fig. 3b): so called large density inversions. In this paper we conventionally define 'mixed layer depth' as the depth at which the temperature difference with respect to the surface is 0.5°C (Jurado et al., 2012). We note that

this actually more represents the 'mixing layer depth' and the reordered profile shows non-zero stratification. If the mixed-layer-depth definition would have been applying a temperature difference of, e.g., 0.001°C on the reordered profile, its value would average about 5 m, much less than using the present and more common, conventional definition applying a temperature difference of 0.5°C. We thus present turbulence results for this commonly defined 'mixed layer' with caution, whilst observing their consistency with the results from deeper down, as presented below. For $-200 < z < -30$ m, large turbulent overturns are few and far between. Turbulence dissipation rate (Fig. 3c) and eddy diffusivity (Fig. 3d) are characterized by relatively small displacement sizes of less than 5 m. For $z < -200$ m, displacement values weakly increase with depth, together with stratification ($\sim N^2$; Fig. 3e). Between $-30 < z < 0$ m, turbulence dissipation rate values between our minimum detectable level 10^{-11} and $>10^{-8}$ m^2 s^{-3} are similar to those found by others, using microstructure profilers (e.g., Oakey, 1982; Gregg, 1989), lowered acoustic Doppler current profiler or CTD-Thorpe scale analysis (e.g., Ferron et al., 1998; Walter et al., 2005; Kunze et al., 2006). Here, eddy diffusivities are found between our minimum detectable $2\text{x}10^{-5}$ and 3×10^{-3} m^2 s^{-1} and these values compare with previous near-surface results (Denman and Gargett, 1983). The relatively small $|d| < 5$ m displacements (Fig. 3b) are genuine turbulent overturns, and they resemble 'Rankine vortices', a common model of cyclones (van Haren and Gostiaux, 2014), as may be best visible in this example in the large turbulent overturn near the surface. The occasional erratic appearance in individual profiles, sometimes still visible in the ten-profile means, reflects smaller overturns in larger ones.

A mid-morning profile at a southern station shows different characteristics (Fig. 4), although 500 m vertically averaged turbulence values are similar to within 10% of those of the northern station. This 10% variation is well within the error bounds of about a factor of two. At this southern station, the near-surface layer is stably stratifying (Fig. 4a) and displays few overturning displacements (Fig. 4b), while the interior demonstrates rarer but occasional intense turbulent overturning (at $z = -160$ m in Fig. 4), presumably due to internal wave

307 breaking. At greater depths, stratification (~N^2; Fig. 4e) weakly decreases, together with ε (Fig.
308 4c) and K_z (Fig. 4d).

309 Latitudinal overviews are given in Fig. 5 for: Average values over the upper z > -15 m,
310 which covers the diurnal mainly convective turbulent mixing range from the surface and under
311 the cautionary note that these waters are weakly, but measurably stratified, average values
312 between -100 < z < -25 m, which covers the seasonal strong stratification, and average values
313 between -500 < z < -100 m, which covers the more permanent moderate stratification. Noting
314 that all panels have a vertical axis representing a logarithmic scale, variations over nearly four
315 orders of magnitude in turbulence dissipation rate (Fig. 5a) and eddy diffusivity (Fig. 5b) are
316 observed between casts at the same station. This variation in magnitude is typically found in
317 near-surface open-ocean turbulence microstructure profiles (e.g., Oakey, 1982). Still,
318 considerable variability over about two orders of magnitude is observed between the averages
319 from the different stations. This variation in station- and vertical averages far exceeds the
320 instrumental error bounds of a factor of two (0.3 on a log-scale), and thus reveals local
321 variability. The turbulence processes occur 'intermittently'.

322 The observed variability over two orders of magnitude between yoyo-casts at a single
323 station may be due to active convective overturning during early morning in the near-
324 homogeneous upper layer, or due to internal wave breaking and sub-mesoscale variability
325 deeper down. Despite the large variability at stations, trends are visible between stations in the
326 upper 100 m over the 33° latitudinal range going poleward: Buoyancy frequency (~ square root
327 of stratification) steadily decreases significantly (p-value < 0.05) given the spread of values at
328 given stations, with the notion that near-surface (-15 < z < 0 m) values show the same latitudinal
329 trend as deeper-down-values across a larger spread of values, while turbulence values vary
330 insignificantly with latitude as they remain the same or weakly increase by about half an order
331 of magnitude (about a factor of 3). At a given depth range, turbulence dissipation rates roughly
332 follow a log-normal distribution with standard deviations well exceeding half an order of
333 magnitude. The comparison of latitudinal variations with the (log-normal) distribution is
334 declared insignificant with p > 0.05 when the mean values are found within 2 standard

deviations (see Appendix A2). This is not only performed for turbulence dissipation rate, but also for other quantities. The trends suggest only marginally larger turbulence going poleward, which is possibly due to larger cooling from above and larger internal wave breaking deeper down. It is noted that the results are somewhat biased by the sampling scheme, which changed from 3 to 4 h after sunrise sampling at high latitudes to 4 to 5 h after sunrise sampling at lower latitudes, see the sampling hours after local sunrise in (Fig. 5d). Its effect is difficult to quantify, but should not show up in turbulence values from deeper down ($-500 < z < -100$ m).

Between $-500 < z < -100$ m, no clear significant trend with latitude is visible in the turbulence values (Fig. 5a,b), although $[K_z]$ weakly increases with increasing latitude at all levels between $-500 < z < 0$ m, while buoyancy frequency significantly decreases (Fig. 5c). The data from well-stratified waters deeper down thus show the same latitudinal trend as the observations from the near-surface layers, even though the latter are less well determined because of the weak stratification. Our turbulence values from CTD-data also confirm previous results by Jurado et al. (2012) who made microstructure profiler observations from the upper $z > -100$ m along the same transect. Their results showed turbulence values remain unchanged over 30º latitude or increase by at most one order of magnitude, depending on depth level. Their 'mixed' layer ($z >\sim -25$ m) turbulence values are similar to our $z > -15$ m values and half to one order of magnitude larger than the present deeper observations. The slight discrepancy in values averaged over $z > -25$ m may point at either i) a low bias due to a too strict criterion of accepting density variations for reordering applied here, or ii) a high bias of the ~10-m largest overturns having similar velocity scales (of about 0.05 m s^{-1}) as their 0.1 m s^{-1} slowly descending SCAMP microstructure profiler. At greater depths, $-500 < z < -100$ m, it is seen in the present observations that the spread in turbulence values over four orders of magnitude at a particular station is also large. This spread in values suggests that dominant turbulence processes show similar intermittency in weakly (at high-latitudes $N \approx 10^{-2.5}$ s^{-1}) and moderately (at mid-latitudes $N \approx 10^{-2.2}$ s^{-1}) stratified waters, respectively, for the given resolution of the instrumentation.

Mean values of N are larger by half an order of magnitude in the seasonal pycnocline (found in the range $-100 < z < -25$ m) than those near the surface and in the more permanent

363 stratification below (Fig. 5). Such local vertical variations in N have the same range of variation
364 as observed horizontally across latitudes [30, 63]° per depth level.
365
366 **3.2 Nutrient distributions and fluxes**
367 Vertical profiles of macro-nutrients generally resemble those of density anomaly in the
368 upper z > -500 m (Fig. 6). In the south, low macro-nutrient values are generally distributed over
369 a somewhat larger near-surface mixed layer. The mixed layer depth, at which temperature
370 differed by 0.5°C from the surface (Jurado et al., 2012), varies between about 20 and 30 m on
371 the southern end of the transect and weakly becomes shallower with latitude (Fig. 7a). This
372 weak trend may be expected from the summertime wind conditions that also barely vary with
373 latitude (Fig. 7b,c). In contrast, the euphotic zone, defined as the depth of the 0.1% irradiance
374 penetration level (Mojica et al., 2015), demonstrates a clear latitudinal trend decreasing from
375 about 150 to 50 m (Fig. 7a). For z < -100 m below the seasonal stratification, vertical gradients
376 of macro-nutrients are large (Fig. 6b-d). Macro-nutrient values become approximately
377 independent of latitude at depths below z < -500 m. Dissolved iron profiles differ from macro-
378 nutrient profiles, notably in the upper layer near the surface (Fig. 6a). At some southern stations,
379 dissolved iron and to a lesser extent also phosphate, have relatively high concentrations closest
380 to the surface. These near-surface concentration increases suggest atmospheric sources, most
381 likely Saharan dust deposition (e.g., Rijkenberg et al., 2012).
382 As a function of latitude in the near-surface 'mixed' layer (Fig. 8), the vertical turbulent
383 fluxes of phosphate (representing the macro-nutrients, for graphical reasons, see the similarity
384 in profiles in Fig.6b-d) are found constant or insignificantly ($p > 0.05$) increasing (Fig. 8d).
385 Here, the mean eddy diffusivity values for the near-surface layer as presented in Fig. 5 are used
386 for computing the fluxes. It is noted that in this layer turbulent overturning (Figs 3b, 4b) is
387 larger and nutrients are mainly depleted (Fig. 6), except when replenished from atmospheric
388 sources in which case gradients reverse sign as in most DFe-profiles. Hereby, lateral diffusion
389 is not considered important. Nonetheless, macro-nutrients are seen to increase significantly
390 towards higher latitudes (Fig. 8b). We note that the vertical gradients in Fig. 8c, in which only

391 downgradient values are plotted, are very weak in general within the standard deviation of
392 measurements. The results in Fig. 8d are thus merely indicative, but they are consistent with
393 the results from deeper down presented below.

394 More importantly, the significant vertical turbulent fluxes of nutrients across the seasonal
395 pycnocline (Fig. 9) are found ambiguously or statistically independently varying with latitude
396 (Fig. 9d). Likewise, the vertical turbulent fluxes of dissolved iron and phosphate are marginally
397 constant with latitude across the more permanent stratification deeper down (Fig. 10). Nitrate
398 fluxes show the same latitudinal trend, with values around 10^{-6} mmol m^{-2} s^{-1}. Overall, the
399 vertical turbulent nutrient fluxes across the seasonal and more permanent stratification resemble
400 those of the physical vertical turbulent mass flux, which is equivalent to the distribution of
401 turbulence dissipation rate and which is latitude-invariant (Fig. 5a).

402

403 **4 Discussion**

404 Practically, the upright positioning CTD while using an adaptation consisting of a custom-
405 made equal-surface inlet worked well to minimize ship-motion effects on variable flow-
406 imposed temperature variations. This improved calculated turbulence values from CTD-
407 observations in general and in near-homogeneous layers in particular. The indirect comparison
408 with turbulence values determined from previous microstructure profiler observations along the
409 same transect (Jurado et al., 2012) confirms the same trends, although occasionally turbulence
410 values were lower (to one order of magnitude in the present study). This difference in values
411 may be due to the time-lapse of 8 years between the observations, but more likely it is due to
412 inaccuracies in one or both methods. It is noted that any ocean turbulence observations cannot
413 be made better than to within a factor of two (Oakey, pers. comm.). In that respect, the standard
414 CTD with the here presented adaptation is a cheaper solution than additional microstructure
415 profiler observations. Although the general understanding, mainly amongst modellers, is that
416 the Thorpe length method overestimates diffusivity (e.g., Scotti, 2015; Mater and
417 Venayagamoorthy, 2015), this view is not shared amongst ocean observers (e.g., Gregg et al.,

418 2018). In the large parameter space of the high Reynolds number environment of the ocean,
419 turbulence properties vary constantly, with an interminglement of convection and shear-
420 induced turbulence at various levels. Given sufficient averaging, and adequate mean value
421 parametrization, the Thorpe length method is not observed to overestimate diffusivity. This
422 property of adequate and sufficient averaging yields similar mean parameter values in recent
423 modelling results estimating a mixing coefficient near the classical bound of 0.2 in stationary
424 flows for a wide range of conditions (Portwood et al., 2019). It is noted that diffusivity always
425 requires knowledge of stratification to obtain a turbulent flux, and it is better to consider
426 turbulence dissipation rate for intercomparison purposes. Nevertheless, future research may
427 perform a more extensive comparison between Thorpe scale analysis data and deeper
428 microstructure profiler data.

429 While our turbulence values are roughly similar to those of others transecting the NE-
430 Atlantic over the entire water depth (Walter et al., 2005; Kunze et al., 2006), the focus in the
431 present paper is on the upper 500 m because of its importance for upper-ocean marine biology.
432 Our study demonstrates a significant decrease of stratification with increasing latitude and
433 decreasing temperature that, however, does not lead to significant variation in turbulence values
434 and vertical turbulent fluxes. Our direct estimates of the turbulent flux of nitrate into the
435 euphotic zone are one to two orders of magnitude less than the previously estimated rate of
436 nitrate uptake for the summer period. Our turbulent flux of nitrate values are of the same order
437 of magnitude as reported by others (Cyr et al., 2015 and references therein). In particular, the
438 Martin et al. (2010) study in the Northeast Atlantic Ocean (at 49°N, 16°W) reported similar
439 vertical nutrient fluxes during summer, which provides confidence in the methods used. The
440 same authors reported that the vertical nitrate flux into the euphotic zone was much lower than
441 the rate of nitrate update at the time. To determine these nitrate uptake rates, they spiked water
442 samples with a minimum of 0.5 μM nitrate, representing ~10% of the ambient nitrate
443 concentration. In our study area, the ambient nitrate concentrations in the euphotic zone were
444 much lower (see also Mojica et al., 2015), implying a higher relative importance of nitrate input
445 to the overall uptake demand. Still, primary productivity in the oligotrophic euphotic zone, as

well as in the high latitude Atlantic, is mainly fueled by recycling (e.g., Gaul et al., 1999; Achterberg et al., 2020) and the supply of new nutrients by turbulent fluxes, however small, provides a welcome addition. Besides nutrient input resulting from vertical turbulent fluxes, there is a role for latitudinal differences through the supply of nutrients by deep mixing events, and depending on the location, also potential upwelling and lateral transport events.

We suggest that internal waves may drive the feed-back mechanism, participating in the subtle balance between destabilizing shear and stable (re)stratification. Molecular diffusivity of heat is about 10^{-7} m^2 s^{-1} in seawater, and nearly always smaller than turbulent diffusivity in the ocean. The average values of K_z during our study were typically 100 to 1000 times larger than molecular diffusivity, which implies turbulent diapycnal mixing drives vertical fluxes despite the relatively slow turbulence compared to surface wave breaking. Depending on the gradient of a substance like nutrients or matter, the relatively slow turbulence may not necessarily provide weak fluxes $-K_z d(\text{substance})/dz$ into the photic zone. In the central North Sea, a relatively low mean value of $K_z = 2\times10^{-5}$ m^2 s^{-1} comparable to values over the seasonal pycnocline here, was found sufficient to supply nutrients across the strong summer pycnocline to sustain the entire late-summer phytoplankton bloom in near-surface waters and to warm up the near-bottom waters by some 3°C over the period of seasonal stratification (van Haren et al., 1999). There, the turbulent exchange was driven by a combination of tidal currents modified by the stratification, shear by inertial motions driven by the Coriolis force (inertial shear) and internal wave breaking. Such drivers are also known to occur in the open ocean, although to an unknown extent.

The here observed (lack of) latitudinal trends of ε, K_z and N yield approximately the same information as the vertical trends in these parameters at all stations. In the vertical for $z < -200$ m, turbulence values of ε and K_z weakly vary with stratification. This is perhaps unexpected and contrary to the common belief of stratification hampering vertical turbulent exchange of matter including nutrients. It is less surprising when considering that increasing stratification is able to support larger shear. Known sources of destabilizing shear include near-inertial internal

waves of which the vertical length-scale is relatively small compared to other internal waves, including internal tides (LeBlond and Mysak, 1978).

The dominance of inertial shear over shear by internal tidal motions (internal tide shear), together with larger energy in the internal tidal waves, has been observed in the open-ocean, e.g. in the Irminger Sea around 60°N (van Haren, 2007). The frequent atmospheric disturbances in that area generate inertial motions and dominant inertial shear. Internal tides have larger amplitudes but due to much larger length scales they generate weaker shear, than inertial motions. Small-scale internal waves near the buoyancy frequency are abundant and may break sparsely in the ocean interior outside regions of topographic influence. However, larger destabilizing shear requires larger stable stratification to attain a subtle balance of 'constant' marginal stability (van Haren et al., 1999). Not only storms but all geostrophic adjustments, such as frontal collapse, may generate inertial wave shear also at low latitudes (Alford and Gregg, 2001), so that overall latitudinal dependence may be negligible. If shear-induced turbulence in the upper ocean is dominant it may thus be latitudinally independent (shallow observations by Jurado et al., 2012; deeper observations in present study). There are no indications that the overall open ocean internal wave field and (sub)mesoscale activities are energetically much different across the mid-latitudes. If internal tide sources would have dominated our observations, clear differences in turbulence dissipation rates would have been found at our station near 48 °N (near the Porcupine Bank), for example, compared with those at other stations.

Summarizing, our study infers that vertical nutrient fluxes did not vary significantly with latitude and stratification. This suggests that predicted changes in the physical environment due to global ocean warming have little effect on vertical turbulent exchange. Supposing that enhanced warming leads to more stable stratification, more internal waves can be supported (LeBlond and Mysak, 1978), which upon breaking can maintain the extent of vertical turbulent exchange and thereby, for example, vertical nutrient fluxes. We thus hypothesize that, from a physical environment perspective, in stratified oligotrophic waters the nutrient input from deeper waters and corresponding summer phytoplankton productivity and growth are not

expected to change (much) with future global warming. We invite future observations and numerical modelling to further investigate this suggestion and associated feed-back mechanisms such as internal wave breaking.

Competing interests. The authors declare that they have no conflict of interest.

Acknowledgements. We thank the master and crew of the R/V Pelagia for their pleasant contributions to the sea-operations. J. van Heerwaarden and R. Bakker made the CTD-modification. We much appreciated the critical comments of the reviewers.

511 APPENDIX A1

512 **Modification of CTD pump-tubing to minimize RAM-effects**

513 The unique pump system on SeaBird Electronics (SBE) CTDs, foremost on their high-
514 precision full ocean depth shipborne and cable-lowered SBE911, minimizes the effects of flow
515 variations (and inversions) past its T-C sensors (SeaBird, 2012). This reduction in flow
516 variation is important because the T-sensor has a slower response than the C-sensor. As data
517 from the latter are highly temperature dependent, besides being pressure dependent, the precise
518 matching of all three sensors is crucial for establishing proper salinity and density
519 measurements, especially across rapid changes in any of the parameters. As flow past the T-
520 sensor causes higher measurement values due to friction at the sensor tip, flow-fluctuations are
521 to be avoided as they create artificial T-variations of about 1 mK s m^{-1} (Larson and Pedersen,
522 1996).

523 However, while the pump itself is one thing, its tubing needs careful mounting as well, with
524 in- and outlet at the same depth level (Sea-Bird, 2012). This is to prevent ram pressure $P = \rho U^2$,
525 for density ρ and flow speed U. Unfortunately, the SBE-manual shows tubing of different
526 diameters, for in- and outlet. Different diameter tubing leads to velocity fluctuations of ±0.5 m
527 s^{-1} past the T-sensor, as was concluded from a simple experiment by van Haren and Laan
528 (2016). The flow speed variations induce temperature variations of ±0.5 mK and are mainly
529 detectable in weakly stratified waters such as in the deep ocean, but also near the surface as
530 observed in the present data. Using tubes of the same diameter opening remedied most of the
531 effect, but only if the surface of the tube-opening is perpendicular to the main CT-motion as in
532 a vertically mounted CTD. If it is parallel to the main motion as in a horizontally mounted CTD,
533 the effect was found to be adverse. The make-shift onboard experiment in van Haren and Laan
534 (2016) has now been cast into a better design (Fig. A1), of which the first results are presented
535 in this paper.

APPENDIX A2

PDFs of vertically averaged dissipation rate in comparison with latitudinal trends

Ocean turbulence dissipation rate generally tends to a nearly log-normal distribution (e.g., Pearson and Fox-Kemper, 2018), so that the probability density function (PDF) of the logarithm of ε-values is normally distributed and can be described by the first two moments, the mean and its standard deviation. It is seen in Fig. A2a that the overall distribution of all present data indeed approaches lognormality, despite the relatively large length-scale used in the computations (cf., Yamazaki and Lueck, 1990). When the data are split into the three depth levels as in Fig. 5a, it is seen that ε in the upper $z > -15$ m layer is not log-normally distributed due to a few outlying high values confirming an ocean state dominated by a few turbulence bursts (Moum and Rippeth, 2009), whereas ε in the deeper more stratified layers is nearly log-normally distributed.

When we compare the mean and standard deviations of the distributions with the extreme values of the latitudinal trends as computed for Fig. 5a it is seen that for none of the three depth levels the extreme values are found outside one standard deviation from the mean value. In fact, for deeper stratified waters the extreme values of the trends are found very close to the mean value. It is concluded that the mean dissipation rate does not show a significant trend with latitude, at all depth levels. The same exercise yields extreme buoyancy frequency values lying outside one standard deviation from the mean values for well-stratified waters, from which we conclude that stratification significantly decreases with latitude. This is inferable from Fig. 5c by investigating the spread of mean values around the trend line.

References

Alford, M. H. and Gregg, M. C.: Near-inertial mixing: Modulation of shear, strain and microstructure at low latitude, J. Geophys. Res., 106, 16,947-16,968, 2001.

Achterberg, E. P.: Trace element biogeochemistry in the high latitude North Atlantic Ocean: seasonal variations and volcanic inputs, Glob. Biogeochem. Cycl.. in press, doi: 10.1029/2020GB006674, 2020.

Charria, G., Theetten, S., Vandermeirsch, F., Yelekçi, Ö and Audiffren, N.: Interannual evolution of (sub)mesoscale dynamics in the Bay of Biscay, Ocean Sci., 13, 777-797, 2017.

Cyr, F., Bourgault, D., Galbraith, P. S. and Gosselin, M.: Turbulent nitrate fluxes inthe Lower St. Lawrence Estuary, Canada, J. Geophys. Res., 120, 2308-2330, doi:10.1002/2014JC010272, 2015.

De Baar, H. J. W. et al.: Titan: A new facility for ultraclean sampling of trace elements and isotopes in the deep oceans in the international Geotraces program, Mar. Chem., 111, 4-21, 2008.

Denman, K. L. and Gargett, A. E.: Time and space scales of vertical mixing and advection of phytoplankton in the upper ocean, Limnol. Oceanogr., 28, 801-815, 1983.

Dillon, T. M.: Vertical overturns: A comparison of Thorpe and Ozmidov length scales, J. Geophys. Res., 87, 9601-9613, 1982.

Ferron, B., Mercier, H., Speer, K., Gargett, A. and Polzin, K.: Mixing in the Romanche Fracture Zone, J. Phys. Oceanogr., 28, 1929-1945, 1998.

Galbraith, P. S. and Kelley, D. E.: Identifying overturns in CTD profiles, J. Atmos. Oc. Technol., 13, 688-702, 1996.

Gargett, A. and Garner, T.: Determining Thorpe scales from ship-lowered CTD density profiles, J. Atmos. Oc. Technol., 25, 1657-1670, 2008.

Gaul, W., Antia, A. N. and Koeve, W.: Microzooplankton grazing and nitrogen supply of phytoplankton growth in the temperate and subtropical northeast Atlantic, Mar. Ecol. Progr. Ser., 189, 93-104, 1999.

Gill, A. E.: Atmosphere-Ocean Dynamics, Academic Press, Orlando, Fl, USA, 662 pp, 1982.

586 Grasshoff, K., Kremling, K. and Ehrhardt, M.: Methods of seawater analysis, Verlag
587 Chemie GmbH, Weinheim, 419 pp, 1983.
588 Gregg, M. C.: Scaling turbulent dissipation in the thermocline, J. Geophys. Res., 94, 9686-
589 9698, 1989.
590 Gregg, M. C., Sanford, T. B. and Winkel, D. P.: Reduced mixing from the breaking of internal
591 waves in equatorial waters, Nature, 422, 513-515, 2003.
592 Gregg, M. C., D'Asaro, E. A., Riley, J. J. and Kunze, E.: Mixing efficiency in the ocean, Ann.
593 Rev. Mar. Sci., 10, 443-473, 2018.
594 Henyey, F. S., Wright, J. and Flatte, S. M.: Energy and action flow through the internal wave
595 field - an eikonal approach, J. Geophys. Res., 91, 8487-8495, 1986.
596 Hernández-Hernández, N. et al.: Drivers of plankton distribution across mesoscale eddies at
597 submesoscale range, Front. Mar. Sci., 7, 667, doi:10.3389/fmars.2020.00667, 2020.
598 Hibiya T., Nagasawa, M. and Niwa, Y.: Latitudinal dependence of diapycnal diffusivity in the
599 thermocline observed using a microstructure profiler, Geophys. Res. Lett., 34, L24602,
600 2007.
601 Huisman, J., Pham Thi, N. N., Karl, D. M. and Sommeijer, B.: Reduced mixing generates
602 oscillations and chaos in the oceanic deep chlorophyll maximum, Nature, 439, 322-325,
603 2006.
604 Jurado, E., van der Woerd, H. J. and Dijkstra, H. A.: Microstructure measurements along a
605 quasi-meridional transect in the northeastern Atlantic Ocean, J. Geophys. Res., 117,
606 C04016, doi:10.1029/2011JC07137, 2012.
607 IOC, SCOR, IAPSO: The international thermodynamic equation of seawater – 2010:
608 Calculation and use of thermodynamic properties, Intergovernmental Oceanographic
609 Commission, Manuals and Guides No. 56, UNESCO, Paris, France, 196 pp, 2010.
610 Johnson, K. S., Gordon, R. M. and Coale, K. H.: What controls dissolved iron concentrations
611 in the world ocean? Mar. Chem., 57, 137-161, 1997.

King, B. et al.: Buoyancy frequency profiles and internal semidiurnal tide turning depths in the oceans, J. Geophys. Res., 117, C04008, 2012, doi:10.1029/2011JC007681.

Klunder, M. B., Laan, P., Middag, R., De Baar, H. J. W. and van Ooijen, J. C.: Dissolved iron in the Southern Ocean (Atlantic sector), Deep-Sea Res. II, 58, 2678-2694, 2011.

Kunze, E., Firing, E., Hummon, J. M., Chereskin, T. K. and Thurnherr, A. M.: Global abyssal mixing inferred from lowered ADCP shear and CTD strain profiles, J. Phys. Oceanogr. 36, 1553-1576, 2006.

Larson, N., Pedersen, A. M.: Temperature measurements in flowing water: viscous heating of sensor tips, Proc. 1st IGHEM Meeting, Montreal, PQ, Canada. [Available online at http://www.seabird.com/technical_references/viscous.htm], 1996.

LeBlond, P. H. and Mysak, L. A.: Waves in the Ocean, Elsevier, Amsterdam NL, 602 pp, 1978.

Lueck, R. G.: Thermal inertia of conductivity cells: Theory, J. Atmos. Oc. Technol., 7, 741-755, 1990.

Mater, B. D., Venayagamoorthy, S. K., St. Laurent, L. and Moum, J. N.: Biases in Thorpe-scale estimates of turbulence dissipation. Part I: Assessments from largescale overturns in oceanographic data, J. Phys. Oceanogr., 45, 2497-2521, 2015.

Martin A. P., et al.: The supply of nutrients due to vertical turbulent mixing: A study at the Porcupine abyssal plain study site in the northeast Atlantic, Deep-Sea Res. II, 57, 1293-1302, 2010.

Mensah, V., Le Menn, M. and Morel, Y.: Thermal mass correction for the evaluation of salinity, J. Atmos. Oc. Tech., 26, 665-672, 2009.

Middag, R., de Baar, H. J. W., Laan, P. and Bakker, K.: Dissolved aluminium and the silicon cycle in the Arctic Ocean, Marine Chemistry, 115, 176-195, 2009.

Mojica, K. D. A. et al.: Phytoplankton community structure in relation to vertical stratification along a north-south gradient in the Northeast Atlantic Ocean, Limnol. Oceanogr., 60, 1498-1521, 2015.

638 Mojica, K. D. A., Huisman, J., Wilhelm, S. W. and Brussaard, C. P. D.: Latitudinal variation
639 in virus-induced mortality of phytoplankton across the North Atlantic Ocean, ISME J., 10,
640 500-513, 2016.
641 Moum, J. N. and Rippeth, T. P.: Do observations adequately resolve the natural variability of
642 oceanic turbulence?, J. Mar. Sys., 77, 409-417, 2009.
643 Murphy, J. and Riley, J. P.: A modified single solution method for the determination of
644 phosphate in natural waters, Anal. Chim. Acta, 27, 31-36, 1962.
645 Oakey, N. S.: Determination of the rate of dissipation of turbulent energy from simultaneous
646 temperature and velocity shear microstructure measurements, J. Phys. Oceanogr., 12, 256-
647 271, 1982.
648 Osborn, T. R.: Estimates of the local rate of vertical diffusion from dissipation measurements,
649 J. Phys. Oceanogr., 10, 83-89, 1980.
650 Pearson, B. and Fox-Kemper, B.: Log-normal turbulence dissipation in global ocean models,
651 Phys. Rev. Lett., 120, 094501, 2018.
652 Portwood, G. D., de Bruyn Kops, S. M. and Caulfield, C. P.: Asymptotic dynamics of high
653 dynamic range stratified turbulence, Phys. Rev. Lett., 122, 194504, 2019.
654 Rijkenberg, M. J. A. et al.: Fluxes and distribution of dissolved iron in the eastern (sub-) tropical
655 North Atlantic Ocean, Glob. Biogeochem. Cycl., 26, GB3004,
656 doi:10.1029/2011GB004264, 2012.
657 Rijkenberg, M. J. A. et al.: “PRISTINE”, a new high volume sampler for ultraclean sampling
658 of trace metals and isotopes, Mar. Chem., 177, 501-509, 2015.
659 Sarmiento, J. L. et al.: Response of ocean ecosystems to climate warming, Glob. Biogeochem.
660 Cycl., 18, doi:10.1029/2003GB002134, 2004.
661 Scotti, A.: Biases in Thorpe-scale estimates of turbulence dissipation. Part II: energetics
662 arguments and turbulence simulations, J. Phys. Oceanogr., 45, 2522-2543, 2015.
663 Sea-Bird: Fundamentals of the TC duct and pump-controlled flow used on Sea-Bird CTDs,
664 Proc. Sea-Bird Electronics Appl. note 38, SBE, Bellevue, WA, USA, 5 pp, 2012.

Smith, W. H. F. and Sandwell, D. T. : Global seafloor topography from satellite altimetry and ship depth soundings, Science 277, 1957-1962, 1997.

Stansfield, K., Garrett, C., Dewey, R.: The probability distribution of the Thorpe displacement within overturns in Juan de Fuca Strait, J. Phys. Oceanogr., 31, 3421-3434, 2001.

Strickland, J. D. H. and Parsons, T. R.: A practical handbook of seawater analysis, First edition, Fisheries Research Board of Canada, Bulletin, 167, 293 pp, 1968.

Thorpe, S. A.: Turbulence and mixing in a Scottish loch, Phil. Trans. Roy. Soc. Lond. A, 286, 125-181, 1977.

van Haren, H.: Tidal and near-inertial peak variations around the diurnal critical latitude, Geophys. Res. Lett., 32, L23611, doi:10.1029/2005GL024160, 2005.

van Haren, H.: Inertial and tidal shear variability above Reykjanes Ridge, Deep-Sea Res. I, 54, 856-870, 2007.

van Haren, H. and Gostiaux, L.: Characterizing turbulent overturns in CTD-data, Dyn. Atmos. Oc., 66, 58-76, 2014.

van Haren, H. and Laan, M.: An in-situ experiment identifying flow effects on temperature measurements using a pumped CTD in weakly stratified waters, Deep-Sea Res. I, 111, 11-15, 2016.

van Haren, H., Maas, L., Zimmerman, J. T. F., Ridderinkhof, H. and Malschaert, H.: Strong inertial currents and marginal internal wave stability in the central North Sea, Geophys. Res. Lett., 26, 2993-2996, 1999.

Walter, M., Mertens, C. and Rhein, M.: Mixing estimates from a large-scale hydrographic survey in the North Atlantic, Geophys. Res. Let., 32, L13605, doi:10.1029/2005GL022471, 2005.

Yamazaki, H. and Lueck, R.: Why oceanic dissipation rates are not lognormal, J. Phys. Oceanogr., 20, 1907-1918, 1990.

Figure 1. Bathymetry map of the Northeast Atlantic Ocean based on the 9.1 ETOPO-1 version of satellite altimetry-derived data by Smith and Sandwell (1997). The numbered circles indicate the CTD stations, at station 17 (x) no turbulence parameter, only nutrient sampling was done. At stations 1 and 2 no DFe-samples were taken, at station 18 no nutrient-samples were taken. Depth contours are at 2500 and 5000 m.

Figure 2. Test of effective removal of ship motions in CTD-data after pump in- and outlet modification. Nearly raw 24 Hz sampled downcast data obtained from northern station 32 (cast 9). Short example time series for the 20-m depth range [10, 30] m. (a) Detrended pressure (blue) and its (negative signed) first time derivative -dp/dt, 2-dbar-smoothed (purple). (b) Detrended temperature. (c) Moderately smoothed (~30 degrees of freedom; dof) spectra of data from the 5 to 500 m depth range. (d) Moderately smoothed (40 dof) coherence between dp/dt and T from c., with dashed line indicating the 95% significance level. (e) Corresponding phase difference.

Figure 3. Upper 500 m of turbulence characteristics computed from downcast density anomaly data applying a threshold of 7×10^{-5} kg m^{-3}. Northern station 29, cast 2. (a) Unordered, 'raw' profile of density anomaly referenced to the surface. (b) Overturn displacements following reordering of the profiles in a. Slopes ½ (solid lines) and 1 (dashed lines) are indicated. (c) Logarithm of dissipation rate computed from the profiles in a., r.m.s. calculated over 7 m intervals. We use the mathematics expression 'lg' for the 10-base logarithm, as given in the ISO 80000 specification. (d) As c., but for eddy diffusivity. (e) Logarithm of buoyancy frequency computed after reordering the profiles of a.

Figure 4. As Fig. 3, but for a southern station. Upper 500 m of turbulence characteristics computed from downcast density anomaly data applying a threshold of 7×10^{-5} kg m^{-3}. Southern station 3, cast 4. (a) Unordered, 'raw' profile of density anomaly referenced to the surface. (b) Overturn displacements following reordering of the profiles in a. Slopes ½

(solid lines) and 1 (dashed lines) are indicated. (c) Logarithm of dissipation rate computed from the profiles in a., r.m.s. calculated over 7 m intervals. (d) As c., but for eddy diffusivity. (e) Logarithm of buoyancy frequency computed after reordering the profiles of a.

Figure 5. Summer 2017 latitudinal transect along 17±5°W of turbulence values for upper 15 m averages (green) and averages between -100 < z < -25 m (blue, seasonal pycnocline) and -500 < z < -100 m (black, more permanent pycnocline) from short yoyos of 3 to 6 CTD-casts. Values are given per cast (o) and station average (heavy circle with x; the size corresponds with ±the standard error for turbulence parameters). (a) Logarithm of dissipation rate. (b) Logarithm of diffusivity. (c) Logarithm of buoyancy frequency (the small symbols have the size of ±the standard error). (d) Hour of sampling after sunrise.

Figure 6. Upper 500 m profiles for stations at three latitudes. (a) Density anomaly referenced to the surface, including profiles from Fig. 3a and 4a. (b) Nitrate plus nitrite. (c) Phosphate. (d) Silicate. (e) Dissolved iron.

Figure 7. Latitudinal transect of near-surface layers and wind conditions measured at stations during the observational survey. (a) Mixed layer depth (x) and euphotic zone (o). (b) Wind speed. (c) Wind direction.

Figure 8. Latitudinal transect of near-surface nutrient concentrations. (a) Dissolved iron measured at depths indicated. Missing values reflect not all depths were sampled. (b) Nitrate plus nitrite (red) and phosphate (blue, scale times 10) measured at depths indicated in a. (c) Logarithm of (very weak within standard deviations of measurements) vertical gradients of dissolved iron in a. (o-red) and phosphate in b. (x-blue). Only downgradient values are shown, which excludes several PO_4- and nearly all DFe-gradient values due to near-surface increased values (*cf*. Fig. 6e, 32°N profile). (d). Upward vertical turbulent

fluxes of phosphate concentration gradients in c. using average surface K_z from Fig. 5b, valid for depth average (here, ~17 m) of depths in a.

Figure 9. As Fig. 8, but for -100 < z < -25 m, with fluxes for ~62 m in d.

Figure 10. As Fig. 8, but for -600 (few nutrients sampled at 500) < z < -100 m, with fluxes for ~350 m in d.

Fig. A1. SBE911 CTD-pump in- and outlet modification following the findings in van Haren and Laan (2016). (a) The T- and C-sensors clamped together with a structure holding in- and outlet pump-tubing of exactly the same diameter, separated at 0.3 m distance in the horizontal plane. (b) The modification of a. mounted in the CTD-frame.

Fig. A2. Probability Density Functions of logarithm of vertically averaged dissipation rate in comparison with latitudinal trend extreme values. (a) Distribution as a function of latitude for all data. (b) As a, but for the upper 15 m averages only. The mean value is given by the vertical purple line, with the horizontal line indicating +/- 1 standard deviation. The vertical light-blue lines indicate the best-fit value of the trend for 30° and 63°N. (c) As b, but for averages between -100 < z < -25 m. (d) As c, but for averages between -500 < z < -100 m.

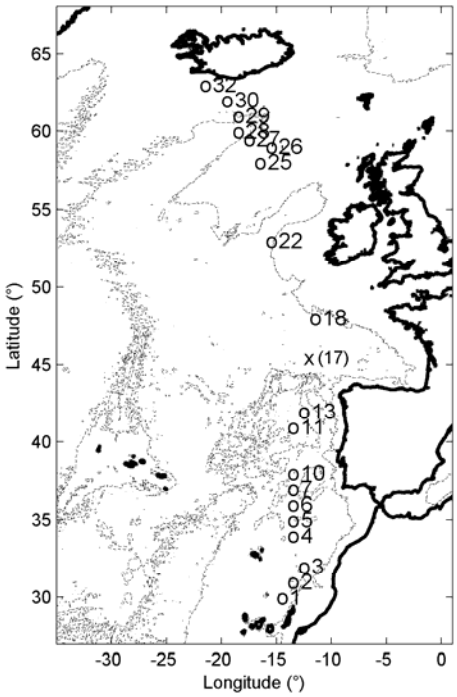

769
770 **Figure 1**. Bathymetry map of the Northeast Atlantic Ocean based on the 9.1 ETOPO-1
771 version of satellite altimetry-derived data by Smith and Sandwell (1997). The numbered
772 circles indicate the CTD stations, at station 17 (x) no turbulence parameter, only nutrient
773 sampling was done. At stations 1 and 2 no DFe-samples were taken, at station 18 no
774 nutrient-samples were taken. Depth contours are at 2500 and 5000 m.
775

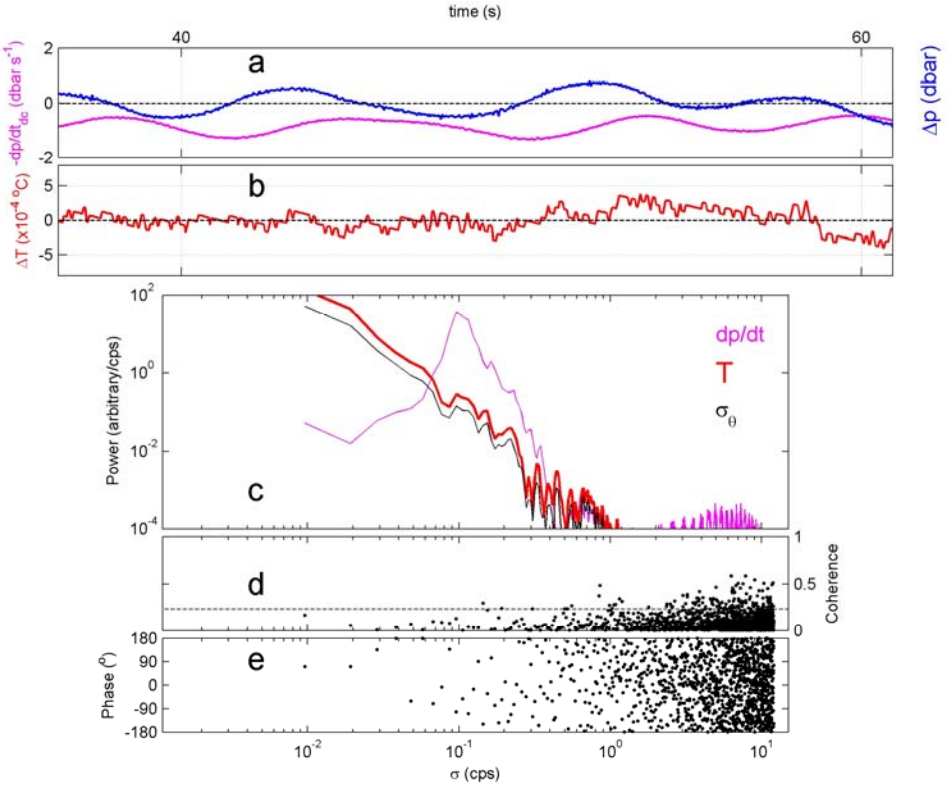

Figure 2. Test of effective removal of ship motions in CTD-data after pump in- and outlet modification. Nearly raw 24 Hz sampled downcast data obtained from northern station 32 (cast 9). Short example time series for the 20-m depth range [10, 30] m. (a) Detrended pressure (blue) and its (negative signed) first time derivative -dp/dt, 2-dbar-smoothed (purple). (b) Detrended temperature. (c) Moderately smoothed (~30 degrees of freedom; dof) spectra of data from the 5 to 500 m depth range. (d) Moderately smoothed (40 dof) coherence between dp/dt and T from c., with dashed line indicating the 95% significance level. (e) Corresponding phase difference.

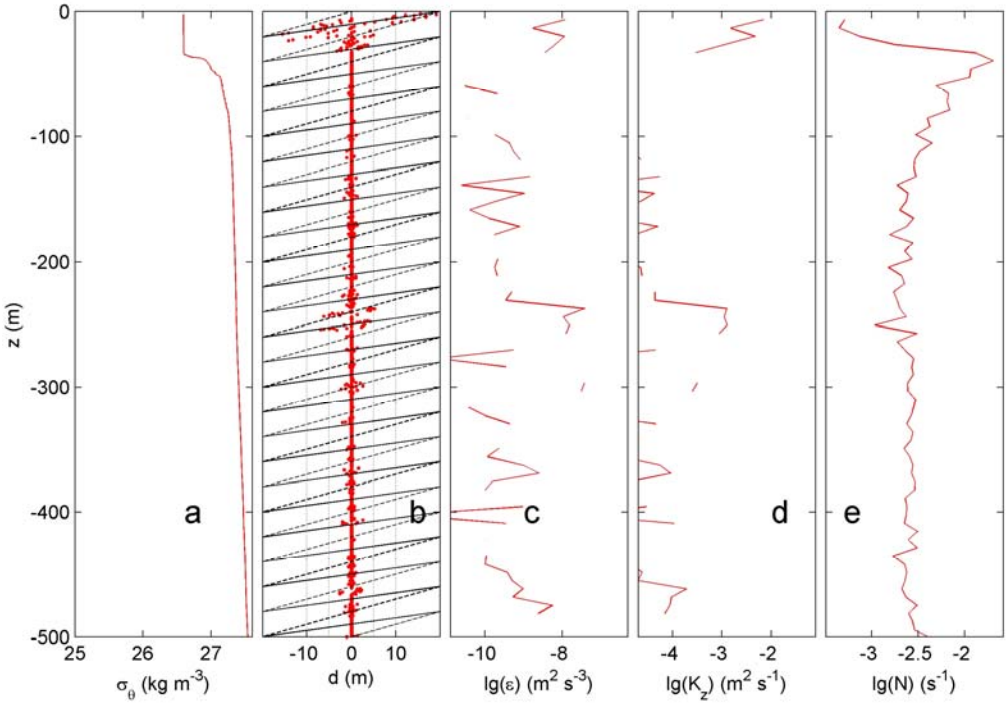

Figure 3. Upper 500 m of turbulence characteristics computed from downcast density anomaly data applying a threshold of 7×10^{-5} kg m^{-3}. Northern station 29, cast 2. (a) Unordered, 'raw' profile of density anomaly referenced to the surface. (b) Overturn displacements following reordering of the profiles in a. Slopes ½ (solid lines) and 1 (dashed lines) are indicated. (c) Logarithm of dissipation rate computed from the profiles in a., r.m.s. calculated over 7 m intervals. We use the mathematics expression 'lg' for the 10-base logarithm, as given in the ISO 80000 specification. (d) As c., but for eddy diffusivity. (e) Logarithm of buoyancy frequency computed after reordering the profiles of a.

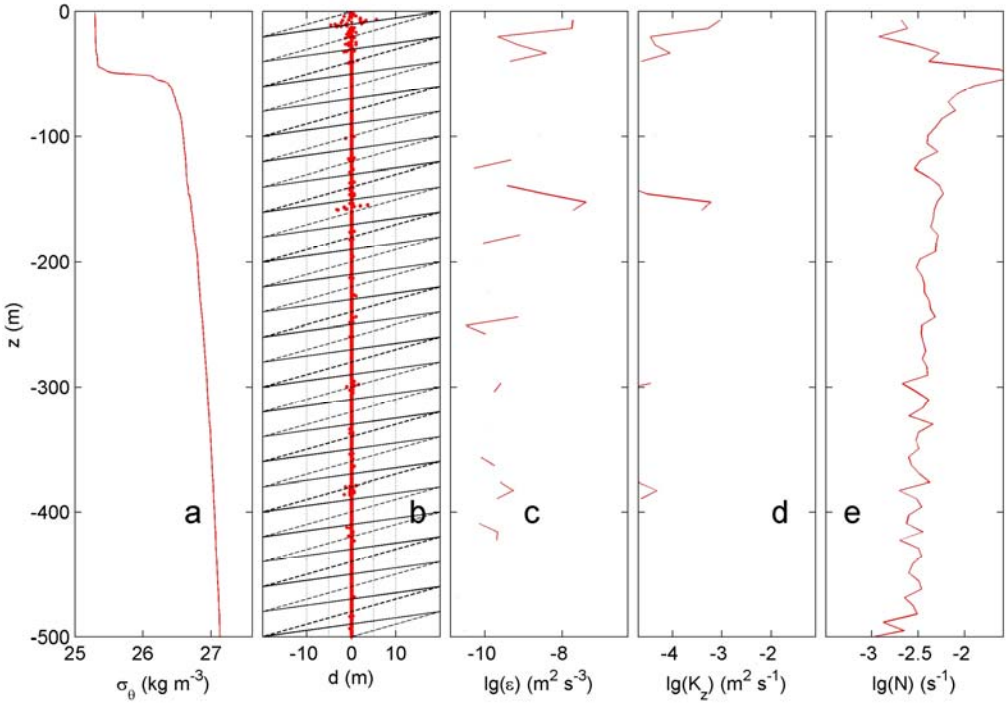

Figure 4. As Fig. 3, but for a southern station. Upper 500 m of turbulence characteristics computed from downcast density anomaly data applying a threshold of 7×10^{-5} kg m^{-3}. Southern station 3, cast 4. (a) Unordered, 'raw' profile of density anomaly referenced to the surface. (b) Overturn displacements following reordering of the profiles in a. Slopes ½ (solid lines) and 1 (dashed lines) are indicated. (c) Logarithm of dissipation rate computed from the profiles in a., r.m.s. calculated over 7 m intervals. (d) As c., but for eddy diffusivity. (e) Logarithm of buoyancy frequency computed after reordering the profiles of a.

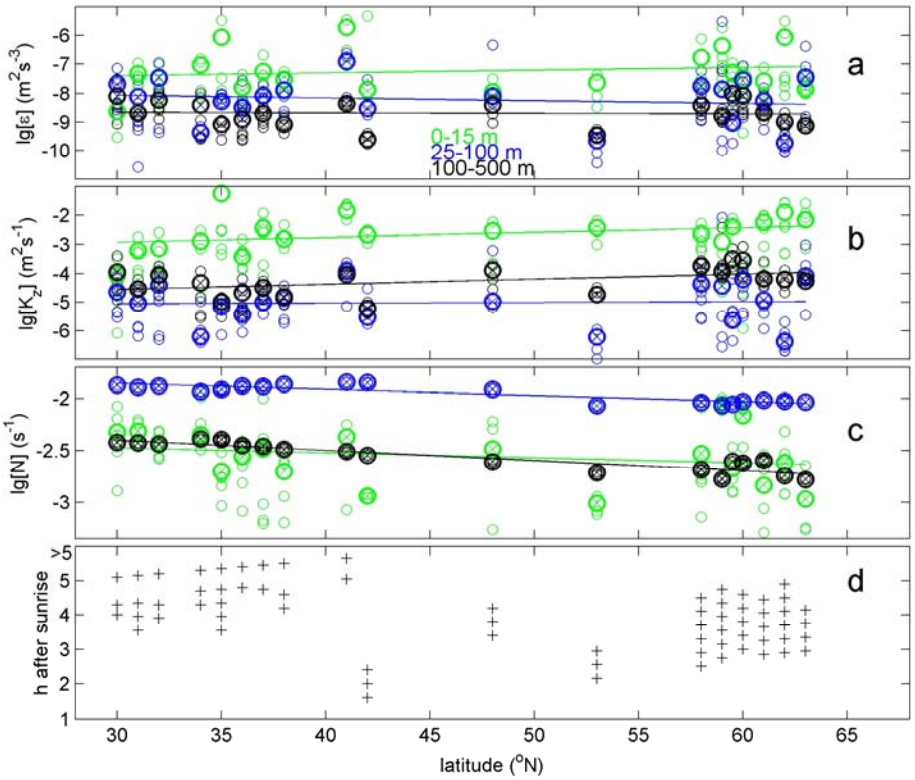

Figure 5. Summer 2017 latitudinal transect along 17±5°W of turbulence values for upper 15 m averages (green) and averages between -100 < z < -25 m (blue, seasonal pycnocline) and -500 < z < -100 m (black, more permanent pycnocline) from short yoyos of 3 to 6 CTD-casts. Values are given per cast (o) and station average (heavy circle with x; the size corresponds with ±the standard error for turbulence parameters). (a) Logarithm of dissipation rate. (b) Logarithm of diffusivity. (c) Logarithm of buoyancy frequency (the small symbols have the size of ±the standard error). (d) Hour of sampling after sunrise.

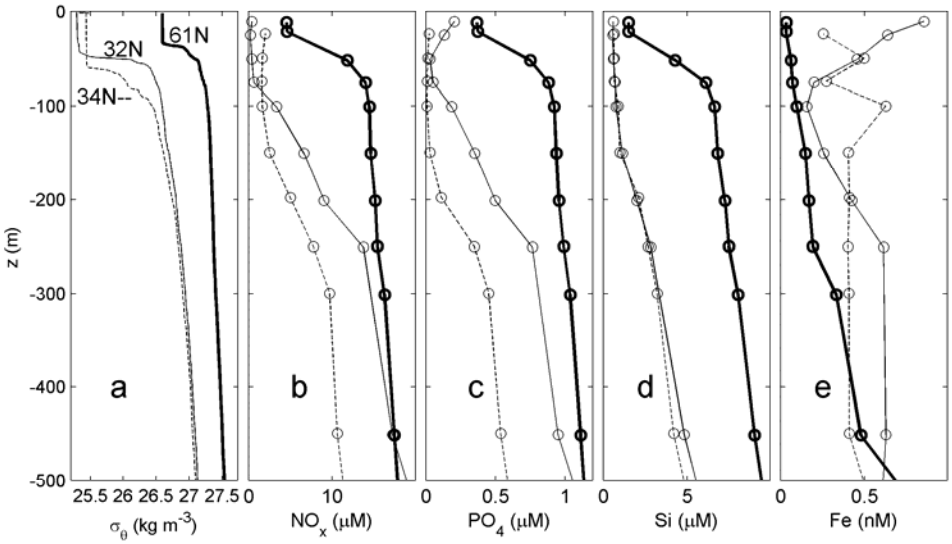

817
818 **Figure 6**. Upper 500 m profiles for stations at three latitudes. (a) Density anomaly
819 referenced to the surface, including profiles from Fig. 3a and 4a. (b) Nitrate plus nitrite. (c)
820 Phosphate. (d) Silicate. (e) Dissolved iron.
821

822

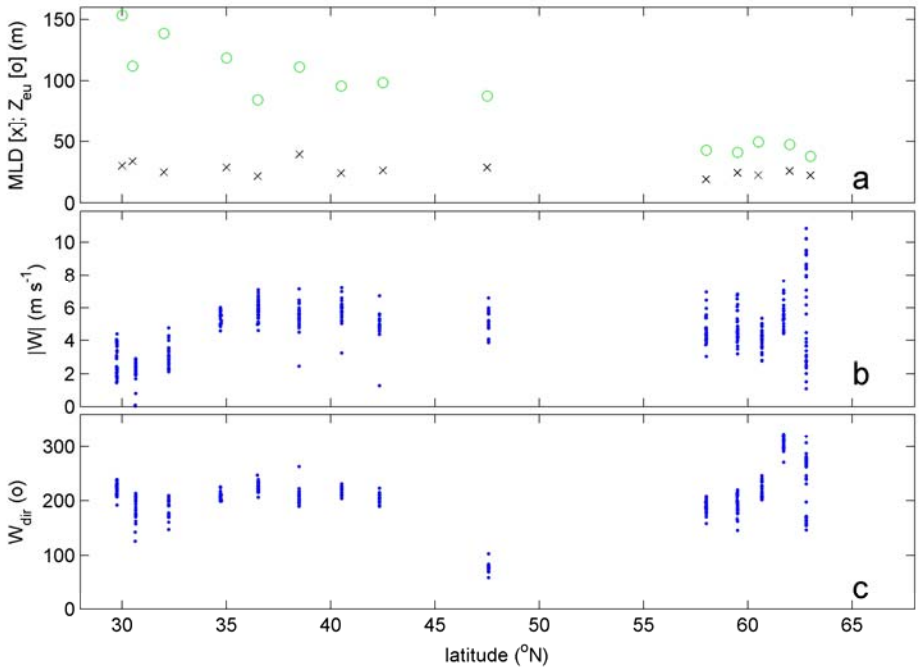

823
824 **Figure 7**. Latitudinal transect of near-surface layers and wind conditions measured at
825 stations during the observational survey. (a) Mixed layer depth (x) and euphotic zone (o).
826 (b) Wind speed. (c) Wind direction.
827

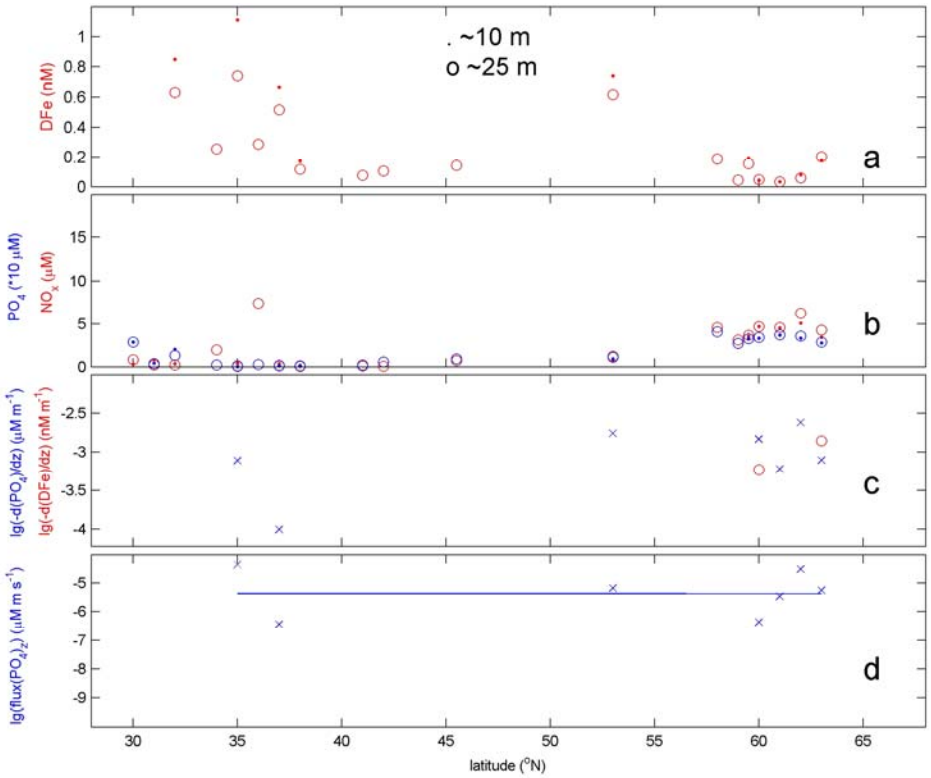

Figure 8. Latitudinal transect of near-surface nutrient concentrations. (a) Dissolved iron measured at depths indicated. Missing values reflect not all depths were sampled. (b) Nitrate plus nitrite (red) and phosphate (blue, scale times 10) measured at the depths indicated in a. (c) Logarithm of (very weak within standard deviations of measurements) vertical gradients of dissolved iron in a. (o-red) and phosphate in b. (x-blue). Only downgradient values are shown, which excludes several PO_4- and nearly all DFe-gradient values due to near-surface increased values (*cf*. Fig. 6e, 32°N profile). (d). Upward vertical turbulent fluxes of phosphate concentration gradients in c. using average surface K_z from Fig. 5b, valid for the depth average (here, ~17 m) of depths in a.

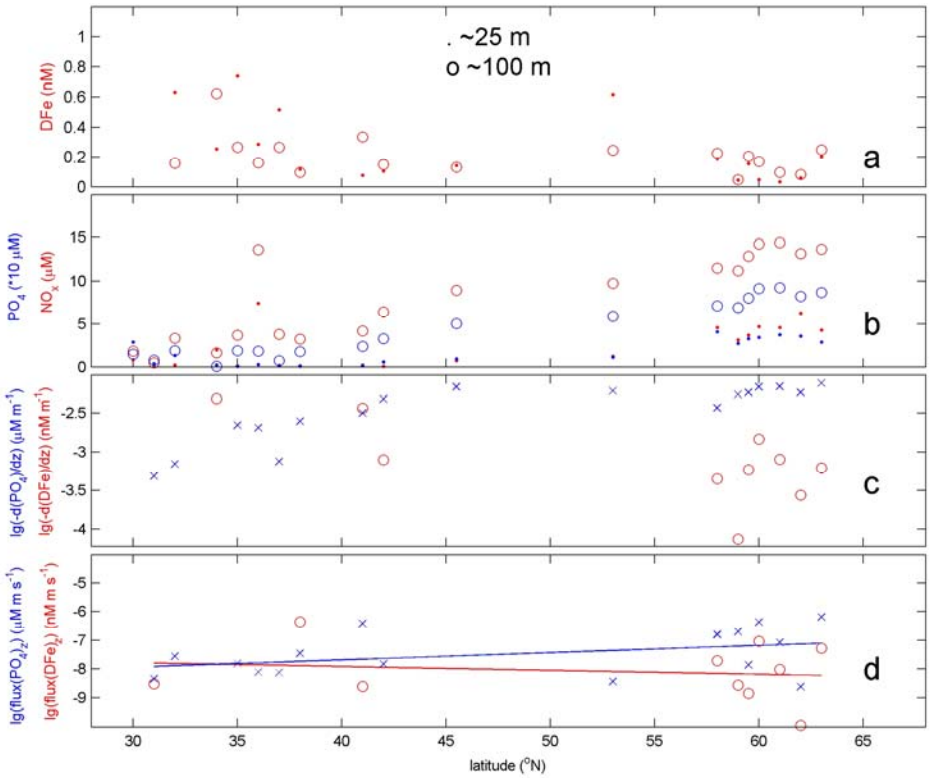

Figure 9. As Fig. 8, but for -100 < z < -25 m, with fluxes for ~62 m in d.

842

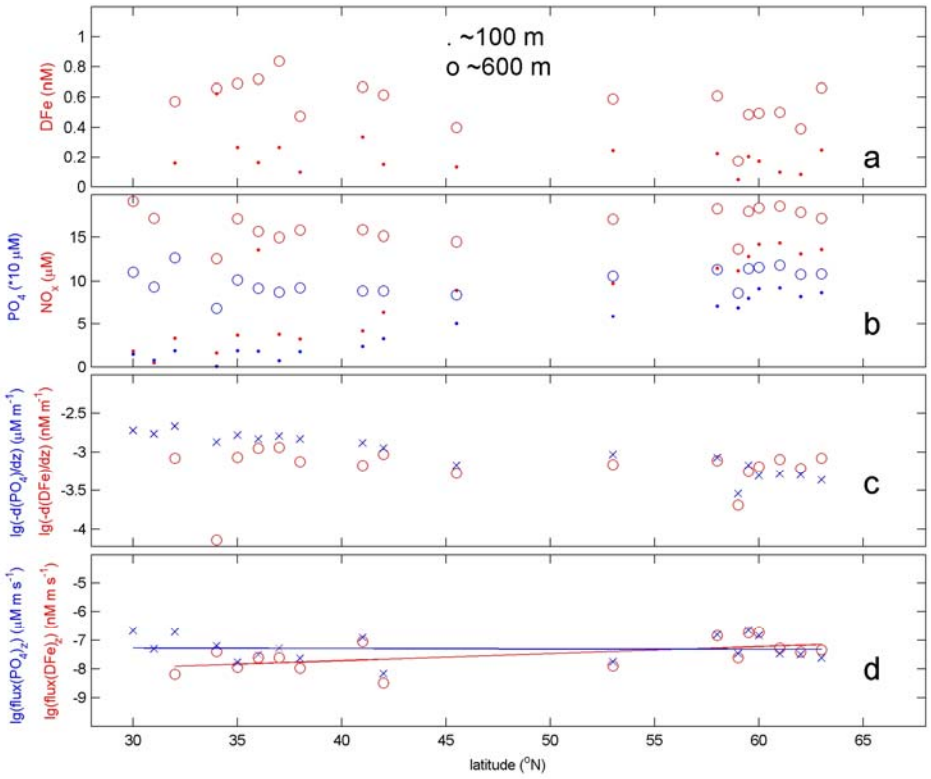

843

844 **Figure 10**. As Fig. 8, but for -600 (few nutrients sampled at 500) < z < -100 m, with fluxes
845 for ~350 m in d.

846

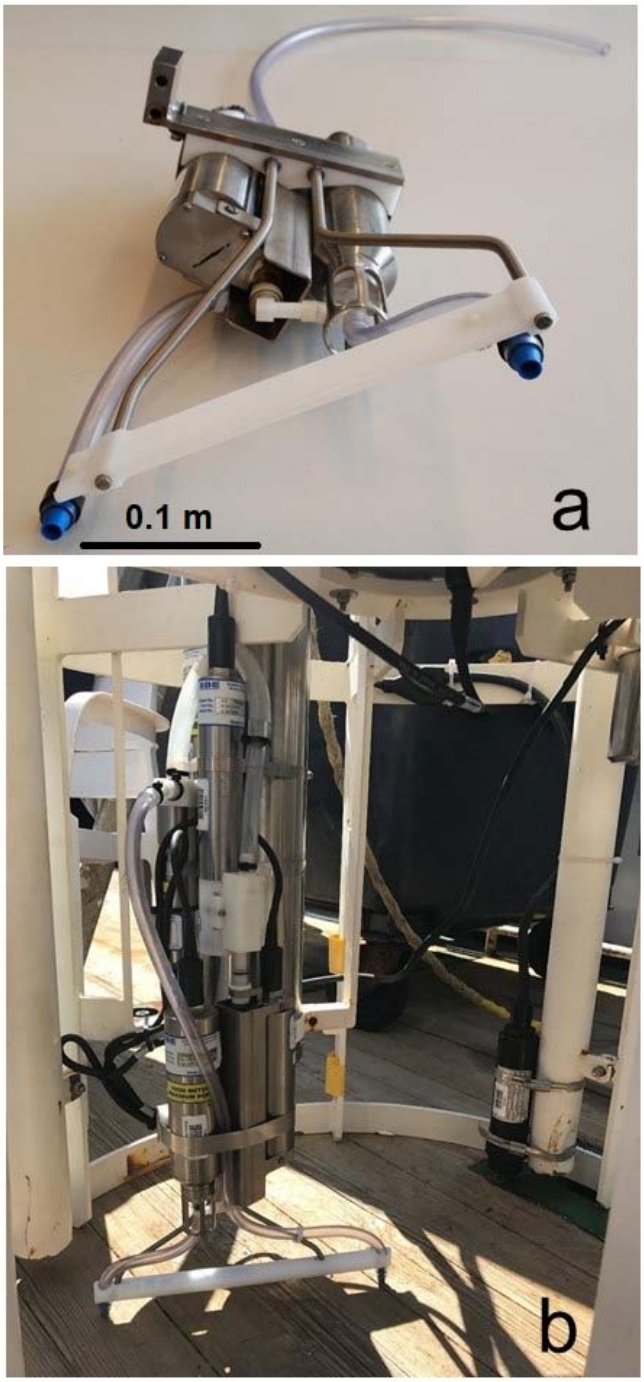

Fig. A1. SBE911 CTD-pump in- and outlet modification following the findings in van Haren and Laan (2016). (a) The T- and C-sensors clamped together with a structure holding in- and outlet pump-tubing of exactly the same diameter, separated at 0.3 m distance in the horizontal plane. (b) The modification of a. mounted in the CTD-frame.

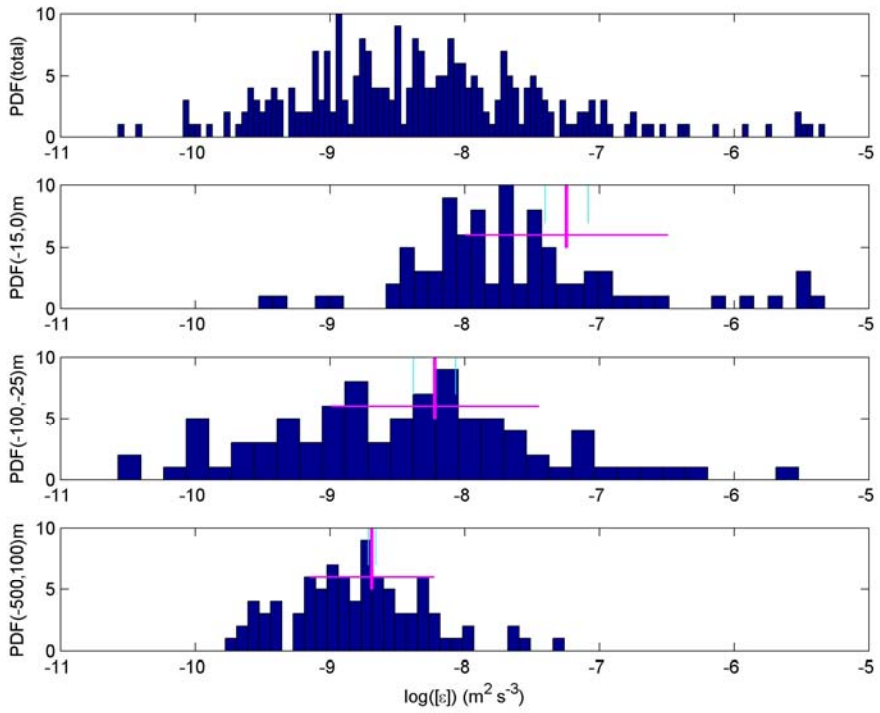

Fig. A2. Probability Density Functions of logarithm of vertically averaged dissipation rate in comparison with latitudinal trend extreme values. (a) Distribution as a function of latitude for all data. (b) As a, but for the upper 15 m averages only. The mean value is given by the vertical purple line, with the horizontal line indicating +/- 1 standard deviation. The vertical light-blue lines indicate the best-fit value of the trend for 30° and 63°N. (c) As b, but for averages between -100 < z < -25 m. (d) As c, but for averages between -500 < z < -100 m.